Journal of Applied Physics

RESEARCH ARTICLE | OCTOBER 23 2024

Sound speed determination in copper shock compressed to 190 GPa

J. A. Hawreliak ; J. M. Winey ; Y. Toyoda ; K. Zimmerman ; Y. M. Gupta

J. Appl. Phys. 136, 165902 (2024)
https://doi.org/10.1063/5.0220264

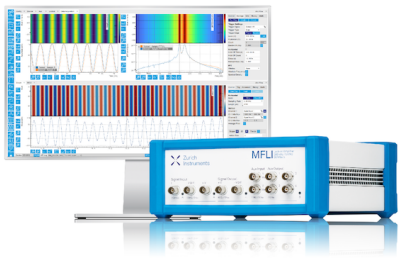

Journal of Applied Physics ARTICLE pubs.aip.org/aip/jap

Sound speed determination in copper shock compressed to 190 GPa

Cite as: J. Appl. Phys. **136**, 165902 (2024); doi: 10.1063/5.0220264
Submitted: 23 May 2024 · Accepted: 7 October 2024 ·
Published Online: 23 October 2024

J. A. Hawreliak,[1] J. M. Winey,[1,a)] Y. Toyoda,[1] K. Zimmerman,[1] and Y. M. Gupta[1,2]

AFFILIATIONS

[1]Institute for Shock Physics, Washington State University, Pullman, Washington 99164-2816, USA
[2]Department of Physics and Astronomy, Washington State University, Pullman, Washington 99164-2814, USA

[a)]**Author to whom correspondence should be addressed:** mwiney@wsu.edu

ABSTRACT

Sound speed measurements in shock compressed solids have long been valuable for the development of equations of state at extreme conditions, shock-induced phase transformations, and a comprehensive characterization of the thermophysical response of high-pressure standards. We present results from plate impact experiments to 190 GPa to determine the longitudinal sound speed in copper—an important high-pressure standard. Surprisingly, the sound speeds determined using the two most common experimental techniques—the front surface impact (FSI) approach and the release wave overtake (RWO) approach—diverge significantly for stresses greater than ~100 GPa. Further analyses, including numerical simulations, show that the FSI experiments provide the correct sound speeds and that fundamental assumptions underlying the RWO method are likely violated due to the complex release response of shock compressed copper. The sound speeds determined using the FSI approach provide for a more accurate high-pressure description of copper in dynamic compression experiments. The present findings are in contrast to the results for shock compressed silver [Wallace *et al.*, Phys. Rev. B **104**, 214106 (2021)], where both methods provided consistent sound speed results. Thus, the findings presented here demonstrate the need to experimentally verify the validity of the RWO method on a case-by-case basis. Finally, we note that even at the high stresses in the present work, the copper unloading response shows a time-dependent, quasielastic response often observed in metals at lower stresses.

I. INTRODUCTION

Development of high-pressure equations of state (EOS) is an essential element of static and dynamic compression science. In particular, experimental determination of the Hugoniot curve (or locus of endstates achievable by shock wave compression) has played a key role in EOS developments at extreme conditions and for the establishment of pressure standards for use in static compression studies[1–3] and impedance matching standards for use in shock compression studies.[4–8] In addition to the Hugoniot response, shock compression studies related to EOS development require an accurate knowledge of the release response from the shocked states.[9,10] Therefore, sound speed determinations in shock compressed materials, which provide information about isentropic compressibility, are important for a comprehensive characterization of the shocked states. More generally, sound speed measurements have long been important for inferring shock-induced phase transformations, including the melt transition, as shown, for example, in the pioneering work on iron.[11,12]

Longitudinal sound speeds in shock compressed solids are typically determined by measuring the propagation velocity of the onset of the release (or rarefaction) waves that unload the material from the shock compressed state. Although release wave speeds can be determined directly using *in situ* stress or particle velocity measurements,[13–16] two other experimental approaches have seen more extensive use. The front surface impact (FSI) method—in which the solid sample is impacted against an optical window (usually LiF)—was used previously for cerium,[17] tantalum,[18] graphite,[19,20] fused silica,[21] magnesium,[22] and silver.[23] This method provides a straightforward approach, but the peak stresses are limited by the maximum impact velocity achievable and the Hugoniot curve of the LiF window.[16] To determine sound speeds at higher stresses, the release wave overtake (RWO) method, pioneered by Brown, McQueen, and coworkers,[11,24] has been used to determine

sound speeds in iron,[11,12,25] tantalum,[26,27] molybdenum,[28,29] beryllium,[30] and silver.[23] Although this method incorporates a more complex experimental configuration, compared to the FSI method, the ability to reach higher stresses enables sound speeds to be determined both below and above the melt transition.[11,12,23,25–30]

Copper is an important high-pressure standard that has been used extensively as a high impedance impactor/buffer in plate impact experiments.[6,7,15,30–32] Cu has also been examined as a standard in ramp compression studies.[33,34] Although the Hugoniot curve for Cu is well established[7,31,35–37] and sound speeds have been reported in the shock-melted liquid phase,[37,38] sound speeds reported for the shock compressed solid phase exhibit significant scatter at stresses below 100 GPa.[38,39] In addition, the reported sound speeds appear to reach a local maximum at stresses near the onset of the face-centered-cubic to body-centered-cubic structural transformation (~180 GPa) reported previously.[40]

To better characterize the response of Cu shock compressed to stresses below melt, we conducted plate impact experiments to determine longitudinal sound speeds using both the FSI and RWO methods for stresses up to 190 GPa. Unexpectedly, the sound speeds determined using the two methods diverge for stresses greater than ~100 GPa. Results from a comprehensive set of experiments and analysis to resolve the differences from the two methods constitute the main elements of this study.

The remainder of the paper is organized as follows. The experimental methods are summarized in Sec. II and the experimental results are presented in Sec. III. In Sec. IV, the results are analyzed to determine sound speeds in shock compressed Cu. The sound speed results, together with the calculated results from numerical simulations, are discussed in Sec. V. A summary of the main findings and the overall conclusions of this study are presented in Sec. VI.

II. EXPERIMENTAL METHODS

The copper samples used in this study were electronic grade, oxygen-free, high conductivity material (OFE C101-00 > 99.99% purity) obtained as polycrystalline rods from ThyssenKrupp. The average ambient density, determined using the Archimedean method, was 8.930 ± 0.003 g/cc. Average longitudinal and shear sound speeds, measured using the pulse-echo technique, were 4.794 ± 0.003 and 2.31 ± 0.01 km/s, respectively. These results are consistent with the published values for OFE copper.[41]

Plate impact experiments to determine sound speeds in shock compressed copper were carried out using the two-stage light gas gun at the Institute for Shock Physics at Washington State University. Similar to previous work on silver,[23] two different experimental approaches were used to determine sound speeds: the front surface impact (FSI) approach and the release wave overtake (RWO) method. The configuration for the FSI experiments is shown in Fig. 1(a). The copper sample was mounted on the projectile and launched against a [100]-oriented lithium fluoride (LiF) window. The impact side of the LiF window was vapor coated with a thin aluminum mirror. Velocity histories were measured using laser interferometry—VISAR (Velocity Interferometer System for Any Reflector[42]) and/or PDV (Photon Doppler Velocimetry[43]). As shown in Fig. 1(a), the wave profile at the impactor/window interface was measured at the center probe using VISAR and/or PDV. We note that the maximum stress reached in the FSI experiments (188 GPa) was determined by the maximum projectile velocity achievable with the two-stage gun and the LiF Hugoniot curve.

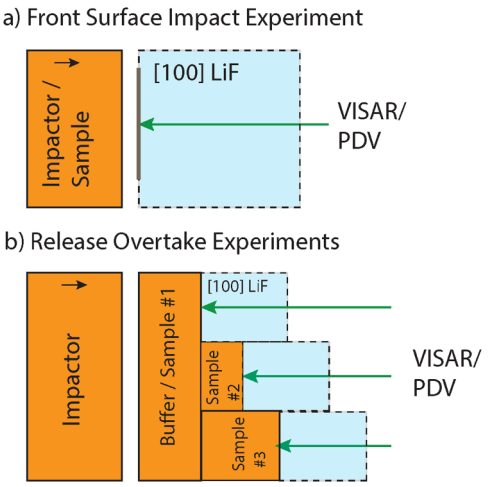

FIG. 1. Experimental configuration for (a) front surface impact (FSI) experiments and (b) release wave overtake (RWO) experiments to measure wave profiles and determine sound speeds in shock compressed Cu.

The RWO experiments used the configuration shown in Fig. 1(b). The target assembly consisted of a Cu buffer and two Cu samples—each having different thickness and backed by a LiF window. These components were bonded together using thin (~1 μm) epoxy bonds, resulting in three different Cu thicknesses for each experiment (nominally between ~0.4 and ~1.5 mm, as measured from the impact surface), which are labeled as I, II, and III in Table I. The target assembly was impacted using a Cu flyer. Particle velocity histories were measured at the Cu/LiF interfaces using laser interferometry (VISAR and PDV). Although the details of the experimental configuration presented here differ somewhat from those of the previous RWO experiments,[11,12,24] we note that the overall approach is similar.

A total of 27 experiments (22 FSI experiments and 5 RWO experiments) are presented here and the relevant experimental parameters are listed in Table I. Although the experiments listed in Table I were conducted over several years, most of them (23 out of 27) have not been reported/published previously.

III. EXPERIMENTAL RESULTS

For both the FSI experiments and the RWO experiments, wave profiles measured at the Cu/LiF interface were corrected for shock-induced changes in the LiF refractive index.[31] In-material shock compressed states for all experiments were determined using the Rankine–Hugoniot jump conditions,[4–6] the measured impactor velocity (Table I), and the reported Hugoniot relations for Cu and LiF (Table II). The results are listed in Table III.

TABLE I. Experimental parameters.

Experiment	Experimental configuration	Cu impactor thickness (μm)	Cu impactor velocity (km/s)	Cu target thickness (μm) I/II/III
1 (17-2s32)	FSI	3002 ± 3	2.706 ± 0.005	…
2 (18-2s07)	FSI	1113 ± 3	3.111 ± 0.002	…
3 (18-2s17)	FSI	1001 ± 3	3.658 ± 0.003	…
4 (18-2s03)	FSI	992 ± 3	4.112 ± 0.010	…
5 (17-2s40)	FSI	997 ± 3	4.603 ± 0.012	…
6 (17-2s38)	FSI	1187 ± 3	4.628 ± 0.016	…
7 (17-2s36)	FSI	1398 ± 3	4.640 ± 0.019	…
8 (17-2s28)	FSI	3016 ± 3	4.641 ± 0.015	…
9 (17-2s46)	FSI	997 ± 3	5.137 ± 0.019	…
10 (19-2s32)	FSI	883 ± 3	5.366 ± 0.003	…
11 (19-2s34)	FSI	870 ± 3	5.404 ± 0.003	…
12 (23-2s07)	FSI	835 ± 3	5.536 ± 0.005	…
13 (18-2sh17)	FSI	902 ± 3	5.756 ± 0.026	…
14 (21-2sh05)[a]	FSI	402 ± 3	6.088 ± 0.007	…
15 (18-2sh20)	FSI	928 ± 3	6.090 ± 0.004	…
16 (21-2sh10)[a]	FSI	392 ± 3	6.825 ± 0.007	…
17 (22-2sh42)	FSI	967 ± 3	6.858 ± 0.010	…
18 (22-2sh34)	FSI	907 ± 4	7.251 ± 0.026	…
19 (21-2sh04)[a]	FSI	357 ± 3	7.307 ± 0.009	…
20 (21-2sh08)[a]	FSI	360 ± 3	7.720 ± 0.005	…
21 (22-2sh35)	FSI	452 ± 5	7.867 ± 0.009	…
22 (23-2sh01)	FSI	298 ± 2	8.267 ± 0.023	…
23 (23-2s15)	RWO	379 ± 3	3.791 ± 0.006	441/881/1320[b,c]
24 (21-2sh45)	RWO	739 ± 3	4.689 ± 0.008	507/995/1495[b,c]
25 (22-2sh25)	RWO	438 ± 3	4.791 ± 0.005	452/889/1337[b,c]
26 (23-2s05)	RWO	364 ± 3	4.853 ± 0.003	450/888/1335[b,c]
27 (23-2s08)	RWO	422 ± 3	5.424 ± 0.006	438/880/1317[b,c]

[a]Experiments reported previously in Ref. 15.
[b]The listed values are the combined thickness of the Cu buffer and the Cu sample for each of the three probe locations in the RWO experiments (Fig. 1).
[c]The listed values have ±0.002 mm uncertainty.

TABLE II. Copper and LiF Hugoniot parameters for $U_S = C_0 + Su_p$.

Material	C_0 (km/s)	S
OFHC copper[a]	3.970 ± 0.017	1.479 ± 0.022
[100] LiF[b]	5.144 ± 0.010	1.355 ± 0.004

[a]Ref. 31.
[b]Ref. 16.

The impact surface velocity profiles measured in the FSI experiments are shown in Fig. 2. In experiments where more than one interferometry probe was used, only a single velocity trace is plotted for visual clarity. To better compare the measured profiles from different experiments, the time axis in Fig. 2 is normalized by the Cu impactor thickness and impact occurs at time zero. For all the FSI experiments, there is a near instantaneous velocity jump at impact, followed by a constant velocity state. The decrease in velocity observed at later times indicates the arrival of the release wave from the back of the impactor. As a representative example, Fig. 2 inset shows how the onset of release (marked with an arrow) was determined.

Figure 3 shows the wave profiles measured for each Cu thickness (labeled I, II, and III) in a representative RWO experiment (experiment 25); the wave profiles measured in the other RWO experiments are similar. Time zero corresponds to the shock wave arrival at the Cu/LiF interface for each sample and the measured particle velocity shows a corresponding abrupt jump to the peak interface velocity. The velocity then remains constant until the arrival of the release wave from the back of the impactor (marked with arrows in Fig. 3). As expected, the duration of the constant state decreases with increasing sample thickness due to the higher velocity of the release wave, compared to the shock wave.

IV. DETERMINATION OF SOUND SPEEDS

For both the FSI and RWO experiments, arrival times (Δt) for the leading edges of the release waves were determined by fitting straight lines to both the constant velocity region of the wave profiles and to the initial portions of the release wave, as shown in the Fig. 2 inset. The intersection of the two fitted lines determined the arrival time. For the FSI experiments, Δt was measured relative to impact. For the RWO experiments, Δt for each Cu thickness was determined relative to the shock wave arrival at the Cu/LiF interface. The measured Δt values for all experiments are listed in Table IV.

Determination of sound speeds from the measured Δt values requires a careful consideration of the wave propagation features encountered in the FSI and RWO experiments. As shown schematically in Fig. 4, these features differ significantly for the two different experimental approaches. In Secs. IV A and IV B, the wave propagation features in the FSI and RWO experiments and the corresponding analysis approaches used to determine sound speeds are discussed in detail.

A. Front surface impact approach

For the FSI experiments (experiments 1–22) shown in Fig. 4(a), the left-going shock wave (red curve) in the Cu impactor reflects as a release wave from the impactor rear surface and propagates through the shock compressed Cu to the impact surface unperturbed by any wave interactions, as shown by the black curve. Therefore, the release wave arrival time (Δt) at the impact surface, shown by the blue dot in Fig. 4(a), is given by

$$\Delta t = \frac{h_{imp}}{U_S} + \frac{h_{imp}}{c_L}, \quad (1)$$

TABLE III. Hugoniot states for shock compressed copper.

Experiment	Impactor velocity (km/s)	Particle velocity (km/s)	Shock velocity (km/s)	Longitudinal stress (GPa)	Density compression ($\rho/\rho_0 - 1$)
1	2.706 ± 0.005	0.825 ± 0.003[a]	5.19 ± 0.02[a]	38.2 ± 0.1	0.189 ± 0.002
2	3.111 ± 0.002	0.955 ± 0.003[a]	5.38 ± 0.02[a]	45.9 ± 0.1	0.216 ± 0.002
3	3.658 ± 0.003	1.133 ± 0.003[a]	5.65 ± 0.03[a]	57.1 ± 0.1	0.251 ± 0.002
4	4.112 ± 0.010	1.281 ± 0.005[a]	5.86 ± 0.03[a]	67.1 ± 0.3	0.280 ± 0.003
5	4.603 ± 0.012	1.443 ± 0.006[a]	6.10 ± 0.03[a]	78.6 ± 0.3	0.310 ± 0.003
6	4.628 ± 0.016	1.451 ± 0.007[a]	6.12 ± 0.03[a]	79.3 ± 0.4	0.311 ± 0.003
7	4.640 ± 0.019	1.455 ± 0.008[a]	6.12 ± 0.03[a]	79.5 ± 0.5	0.312 ± 0.003
8	4.641 ± 0.015	1.455 ± 0.007[a]	6.12 ± 0.03[a]	79.6 ± 0.4	0.312 ± 0.003
9	5.137 ± 0.019	1.619 ± 0.008[a]	6.36 ± 0.03[a]	92.0 ± 0.5	0.341 ± 0.004
10	5.366 ± 0.003	1.695 ± 0.005[a]	6.48 ± 0.03[a]	98.1 ± 0.3	0.355 ± 0.004
11	5.404 ± 0.003	1.708 ± 0.006[a]	6.50 ± 0.03[a]	99.1 ± 0.3	0.357 ± 0.004
12	5.536 ± 0.005	1.752 ± 0.006[a]	6.56 ± 0.03[a]	102.6 ± 0.3	0.364 ± 0.004
13	5.756 ± 0.026	1.825 ± 0.010[a]	6.67 ± 0.04[a]	108.7 ± 0.8	0.377 ± 0.005
14	6.088 ± 0.007	1.935 ± 0.007[a]	6.83 ± 0.04[a]	118.1 ± 0.4	0.395 ± 0.005
15	6.090 ± 0.004	1.936 ± 0.007[a]	6.83 ± 0.04[a]	118.1 ± 0.3	0.395 ± 0.005
16	6.825 ± 0.007	2.182 ± 0.008[a]	7.20 ± 0.04[a]	140.2 ± 0.4	0.435 ± 0.006
17	6.858 ± 0.010	2.193 ± 0.008[a]	7.21 ± 0.04[a]	141.2 ± 0.5	0.437 ± 0.006
18	7.251 ± 0.026	2.324 ± 0.012[a]	7.41 ± 0.04[a]	153.7 ± 0.9	0.457 ± 0.006
19	7.307 ± 0.009	2.343 ± 0.009[a]	7.44 ± 0.04[a]	155.6 ± 0.5	0.460 ± 0.006
20	7.720 ± 0.005	2.482 ± 0.009[a]	7.64 ± 0.05[a]	169.3 ± 0.5	0.481 ± 0.007
21	7.867 ± 0.009	2.531 ± 0.009[a]	7.71 ± 0.05[a]	174.3 ± 0.6	0.488 ± 0.007
22	8.267 ± 0.023	2.665 ± 0.012[a]	7.91 ± 0.05[a]	188.3 ± 1.0	0.508 ± 0.007
23	3.791 ± 0.006	1.896 ± 0.003[b]	6.77 ± 0.05[c]	114.7 ± 0.8	0.389 ± 0.004
24	4.689 ± 0.008	2.344 ± 0.004[b]	7.34 ± 0.08[c]	155.7 ± 1.2	0.460 ± 0.005
25	4.791 ± 0.005	2.396 ± 0.003[b]	7.48 ± 0.03[c]	160.7 ± 1.2	0.468 ± 0.005
26	4.853 ± 0.003	2.426 ± 0.002[b]	7.56 ± 0.06[c]	163.8 ± 1.3	0.473 ± 0.005
27	5.424 ± 0.006	2.712 ± 0.003[b]	7.98 ± 0.06[c]	193.3 ± 1.5	0.515 ± 0.006

[a]Determined using the measured impactor velocity (Table I) and the Hugoniot curves for Cu and LiF (Table II).
[b]The listed value is half of the measured impactor velocity (Table I).
[c]Determined using the Hugoniot curve for Cu (Table II).

where h_{imp} is the Cu impactor thickness, U_S is the shock velocity, and c_L is the Lagrangian release wave speed in the shock compressed Cu. Because h_{imp}, U_S, and Δt are known from the experiment, c_L can be determined by solving Eq. (1). The Eulerian sound speed (the longitudinal sound speed in the shocked state) can be determined from c_L by accounting for the sample thickness change due to compression

$$c_E = c_L \frac{\rho_0}{\rho}, \tag{2}$$

where ρ is the density in shocked Cu.

B. Release wave overtake method

For the RWO approach (experiments 23–27), wave propagation is more complex than for the FSI experiments. Figures 4(b)–4(d) show the position–time plots for wave propagation for each of the three samples for the RWO configuration. In each case, counter propagating shock waves in the sample and the impactor are generated upon impact. When the left-going shock (red curve) in the impactor reaches the rear surface, a right-going release wave (black curve) is generated that propagates back into the impactor and the sample. In addition, when the right-going shock wave in the sample (red curve) reaches the Cu–LiF interface (red dot), a reflected release wave is generated because the LiF window has a lower shock impedance than the Cu sample. The interaction of the two release waves—before the right-going release wave reaches the Cu–LiF interface—is indicated schematically by the yellow circle. We note that, because only the leading edge of the release waves are shown in Fig. 4, the actual release wave interaction is more complex than that shown in the figure. In particular, because the release waves propagate as rarefaction fans,[44,45] the wave interaction occurs over an extended time and distance in the sample (see Appendix for a detailed discussion). This interaction alters the velocity of the right-going release wave over the remaining distance to the interface, shown by the gray curve. The leading edge of the right-going release wave then reaches the Cu–LiF interface at a time indicated by the blue dots in Figs. 4(b)–4(d).

Because the velocity of the right-going release wave is altered by the interaction with the left-going release wave (yellow circle),

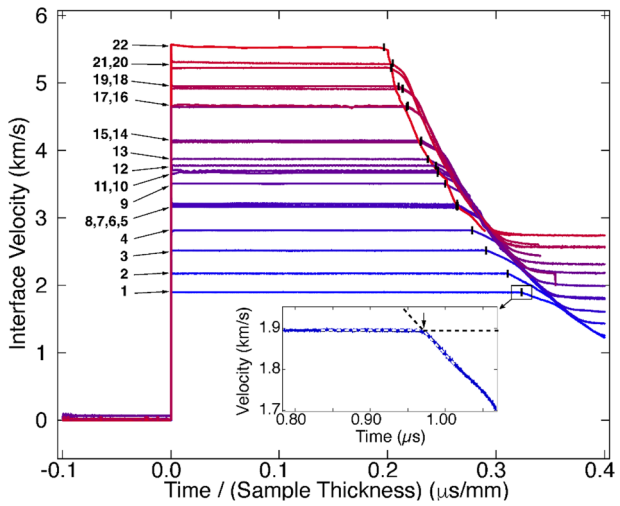

FIG. 2. Measured wave profiles at the impact surface for the front surface impact (FSI) experiments (experiments 1–22). The onset of release is marked with black vertical lines. To better compare wave profiles from different experiments, the time axis is normalized by the Cu impactor thickness. Time zero denotes impact. The color change from blue to red indicates increasing peak stress. The inset shows the onset of release (marked with an arrow) for experiment 1. The two dashed straight lines in the inset are fits to the constant velocity region of the wave profile and to the initial portion of the release wave. The intersection of the two fitted lines determines the release wave arrival time.

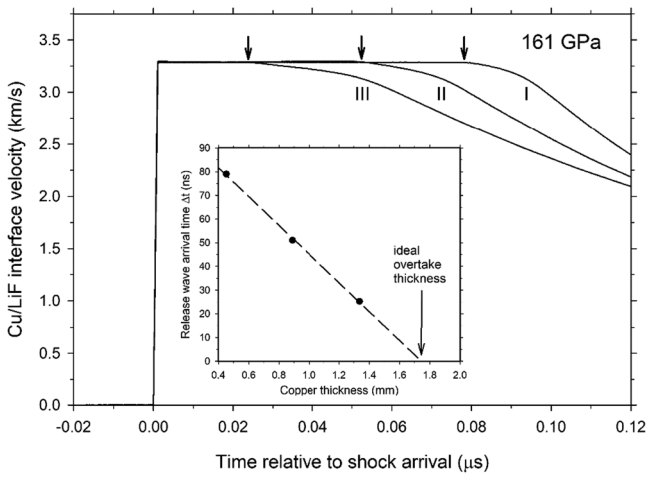

FIG. 3. Measured wave profiles at the Cu/LiF interface for each Cu thickness (labeled I, II, and III, see Table I) in a representative RWO experiment (experiment 25). For each profile, time zero denotes the shock wave arrival at the Cu/LiF interface and the arrows indicate the release wave arrival. The inset shows a straight line fit to the three release wave arrival times to determine the ideal overtake thickness.

the sound speed in shocked Cu cannot be determined directly from the release wave arrival time (blue dot) measured for any of the three individual Cu sample thicknesses. Instead, the effect of the release wave interactions—specifically the change in release wave velocity (gray curve)—must be accounted for. This is not easily accomplished due to the complexity of the wave interactions. However, if certain assumptions (discussed below) regarding the Cu release response are valid, then changes in release wave velocity can be accounted for using an approach similar to that described by Brown and McQueen[11] and McQueen and coworkers,[24] and summarized next.

Figure 4(e) shows the ideal case in which the thickness of the Cu sample is such that the right-going shock wave (red curve) and the right-going release wave (black curve) reach the Cu–LiF interface at the same time ($\Delta t = 0$); the ideal overtake point is indicated by the green dot. In this special case, there are no wave interactions and the Lagrangian release wave velocity c_L can be determined by solving

$$\frac{h_{ov}}{U_S} = \frac{h_{imp}}{U_S} + \frac{h_{imp}}{c_L} + \frac{h_{ov}}{c_L}, \tag{3}$$

where h_{ov} is the ideal overtake thickness of the Cu target, h_{imp} is the impactor thickness, and U_S is the shock velocity. Thus, for a given h_{imp} and U_S, c_L is fully determined by determining the ideal overtake thickness h_{ov}.

Since the ideal overtake thickness is not known in advance, h_{ov} was determined by combining the results from all three sample thicknesses in the following manner. Δt values were determined from the difference between the release wave arrival time [blue dots in Figs. 4(b)–4(e)] and the shock wave arrival time [red dots in Figs. 4(b)–4(e)] for each of the three wave profile measurements, corresponding to the three different target thicknesses (Table I). The three measured Δt values (listed in Table IV) were plotted as a function of the target thickness, as shown in Fig. 3 (inset), and a straight line was fit to the results. Extrapolation of the straight line to $\Delta t = 0$ provided the desired h_{ov} value—similar to the extrapolation shown schematically in Fig. 4(e). Having determined h_{ov}, the Lagrangian sound speed c_L and the Eulerian sound speed c_E were obtained using Eqs. (3) and (2), respectively. We emphasize that—due to the wave interactions—no single sample thickness provides the sound speed. Instead, Δt results for different thicknesses are used to obtain the ideal overtake thickness.

The validity of the linear extrapolation indicated above depends on several fundamental assumptions (discussed in Sec. V A). In particular, a key assumption—not explicitly stated in the literature until recently[23]—is that details of the wave interaction [yellow circles in Figs. 4(b)–4(d)] between the right-going release wave in the sample and the left-going reflection from the sample/window interface are independent of the sample thickness. Expressed differently, the shocked sample is assumed to follow the same stress–volume release path, regardless of the width and location of the wave interaction region. Except for silver,[23] the validity of this assumption for shock compressed solids has not been examined previously. As shown in Sec. V A, this assumption does not hold for the release response of shock compressed copper.

TABLE IV. Sound speeds for shock compressed copper.

Experiment	Longitudinal stress (GPa)	Release wave arrival time, Δt (ns)	Cu overtake thickness (μm)	Lagrangian sound speed (km/s)	Eulerian sound speed (km/s)
1	38.2 ± 0.1	971.2 ± 0.8		7.64 ± 0.05	6.43 ± 0.04
2	45.9 ± 0.1	345.7 ± 0.6		8.01 ± 0.08	6.59 ± 0.06
3	57.1 ± 0.1	291.0 ± 0.6		8.80 ± 0.10	7.04 ± 0.07
4	67.1 ± 0.3	275.6 ± 0.8		9.32 ± 0.12	7.28 ± 0.09
5	78.6 ± 0.3	263.3 ± 0.8		9.97 ± 0.14	7.62 ± 0.10
6	79.3 ± 0.4	313.8 ± 0.7		9.92 ± 0.12	7.56 ± 0.08
7	79.5 ± 0.5	369.2 ± 0.8		9.92 ± 0.12	7.57 ± 0.08
8	79.6 ± 0.4	794.1 ± 0.8		10.01 ± 0.09	7.63 ± 0.05
9	92.0 ± 0.5	252.4 ± 1.1		10.42 ± 0.17	7.77 ± 0.12
10	98.1 ± 0.3	217.2 ± 0.6		10.92 ± 0.16	8.06 ± 0.11
11	99.1 ± 0.3	214.3 ± 0.7		10.83 ± 0.16	7.98 ± 0.11
12	102.6 ± 0.3	204.2 ± 1.2		10.87 ± 0.22	7.96 ± 0.15
13	108.7 ± 0.8	213.8 ± 0.6		11.49 ± 0.17	8.35 ± 0.12
14	118.1 ± 0.4	92.6 ± 0.7		11.92 ± 0.36	8.54 ± 0.25
15	118.1 ± 0.3	214.4 ± 0.6		11.81 ± 0.18	8.46 ± 0.11
16	140.2 ± 0.4	85.3 ± 0.7		12.72 ± 0.41	8.87 ± 0.28
17	141.2 ± 0.5	211.3 ± 0.6		12.53 ± 0.19	8.72 ± 0.11
18	153.7 ± 0.9	193.9 ± 0.7		12.70 ± 0.23	8.72 ± 0.15
19	155.6 ± 0.5	75.0 ± 0.7		13.24 ± 0.50	9.07 ± 0.33
20	169.3 ± 0.5	73.2 ± 0.7		13.83 ± 0.53	9.34 ± 0.35
21	174.3 ± 0.6	92.5 ± 0.7		13.35 ± 0.51	8.97 ± 0.34
22	188.3 ± 1.0	58.6 ± 0.6		14.27 ± 0.50	9.46 ± 0.32
23	114.7 ± 0.8	75.5/47.0/18.5[a,b]	1610 ± 4[c]	10.95 ± 0.09	7.88 ± 0.08
24	155.7 ± 1.2	151.8/122.9/95.7[a,b]	3156 ± 5[c]	11.99 ± 0.13	8.21 ± 0.11
25	160.7 ± 1.2	79.0/51.0/25.2[a,b]	1746 ± 2[c]	12.45 ± 0.12	8.48 ± 0.10
26	163.8 ± 1.3	62.0/35.0/8.0[a,b]	1468 ± 8[c]	12.54 ± 0.11	8.52 ± 0.10
27	193.3 ± 1.5	74.0/48.0/24.5[a,b]	1735 ± 13[c]	13.11 ± 0.12	8.66 ± 0.11

[a]Defined as the time interval between shock wave arrival and release wave arrival for the three Cu thicknesses I/II/III (Table I).
[b]The listed values have ± 0.5 ns uncertainty.
[c]The overtake thicknesses are measured from the impact surface.

C. Copper sound speed results

Lagrangian release wave speeds c_L and Eulerian sound speeds c_E determined from the FSI and RWO experiments on Cu are listed in Table IV, and the Eulerian sound speeds are plotted as a function of density compression ($\mu = \rho/\rho_0 - 1$) in Fig. 5; stresses corresponding to the density compressions are shown on the top of the figure. Results from the FSI experiments show a linear increase with compression, which are fitted well using

$$c_E = (4.79 \pm 0.05) + (9.1 \pm 0.3)\mu \,(\text{km/s}). \quad (4)$$

In contrast, the RWO results show a nonlinear increase, resulting in measurably lower sound speeds compared to the FSI results for compressions greater than $\mu \sim 0.36$ (100 GPa). The differences increase with compression, reaching 11% at 193 GPa. The significant divergence between the FSI results and the RWO results at high stresses was unexpected because the accuracy of both experimental approaches had not been questioned previously in the literature.

Hayes *et al.*[38] reported Cu sound speeds obtained using the RWO method; their results are also shown in Fig. 5. Although their experimental approach used a different variation of the RWO method,[11,24] the previous RWO results at high stresses are in good overall agreement with the RWO results presented here. A quadratic fit, shown in Fig. 5, provides a good match to all the RWO results. For $\mu < 0.35$, the uncertainty band for the fit (blue shaded region) is large due to the large scatter in data at these lower compressions.

Recent Cu sound speed results by Edwards *et al.*,[39] though showing scatter, are in general agreement with the present and previous[38] RWO results (Fig. 5). Although the experimental configuration and the analysis approach differed from the RWO method, we note that the approach in Ref. 39 shared the following attributes with the RWO method: a correction for release wave interactions was required, and the analysis approach used in Ref. 39 was based on underlying assumptions about release wave interactions and material response that are similar to those required by the RWO method. Therefore, the general agreement between the results in Ref. 39 and those from the RWO method is not surprising. We are unable to comment on the scatter in the previous results.

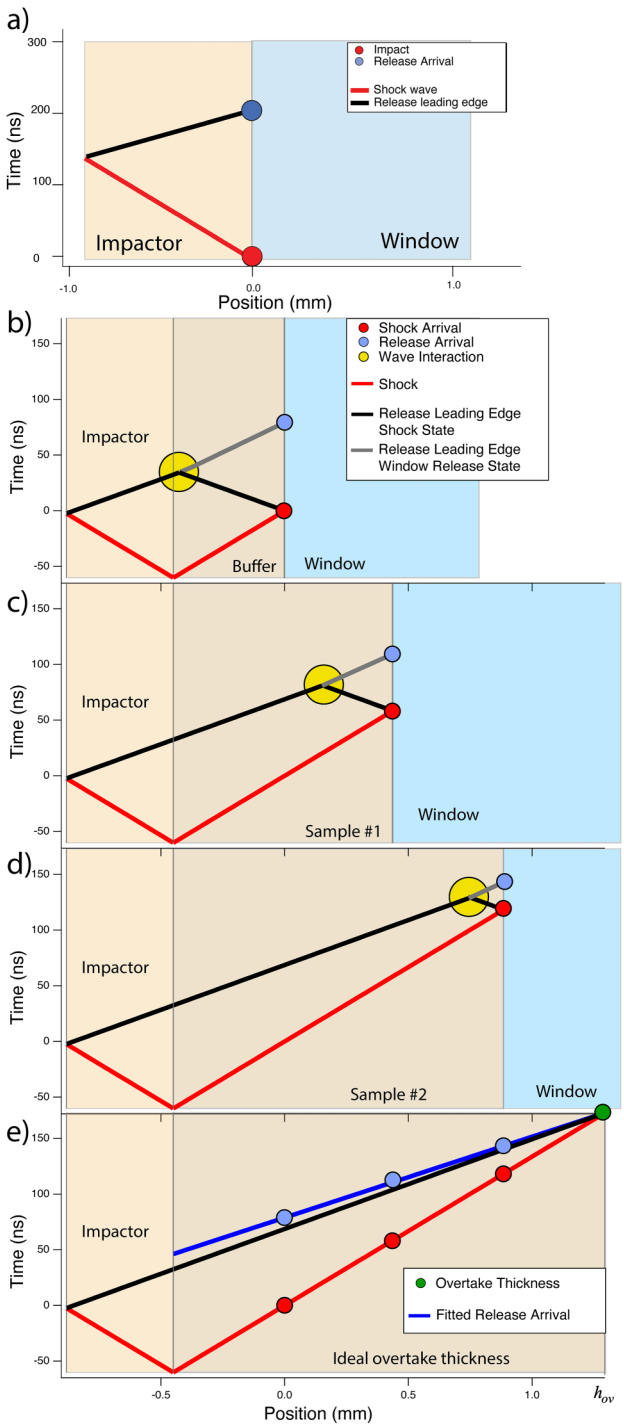

FIG. 4. Time–distance diagrams for (a) front surface impact (FSI) experiments and (b)–(e) release wave overtake (RWO) experiments. The red curves indicate shock waves and the black curves indicate release waves propagating in the shocked sample. The gray curves indicate release waves that have been perturbed by wave interactions. For visual clarity, only the leading edge of the release waves is shown.

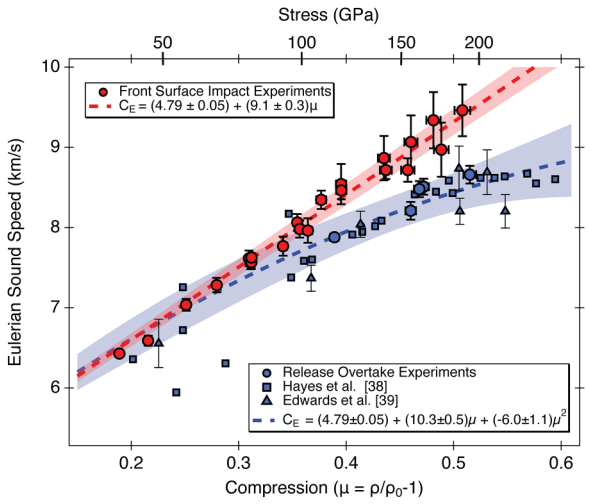

FIG. 5. Sound speed vs density compression for shock compressed copper. The red and blue filled circles are the present FSI and RWO results, respectively. The square and inverted triangles symbols are results from Hayes *et al.*[38] and Edwards *et al.*,[39] respectively. The red curve is a linear fit to the present FSI results. The blue curve is a quadratic fit to the present and previous[38] RWO results. The red and blue shaded regions show uncertainty bands for the FSI fit and the RWO fit, respectively, which incorporate the effects of correlation between the fit parameters. For the RWO results, outlier data points having greater than 3σ deviation from the quadratic fit were not incorporated in the fit.

The present and previous results shown in Fig. 5 suggest that the significant differences between the FSI results and the RWO results at high stresses are associated with the experimental approaches and are not the result of experimental errors. Potential reasons for these differences are discussed next.

V. DISCUSSION

The significantly different sound speeds determined from the FSI experiments and the RWO experiments, as shown in Fig. 5, raise the question: Which experimental approach provides the correct sound speeds for shock compressed Cu?

The following factors support the FSI approach over the RWO method. With the FSI approach, the release wave from the impactor rear surface propagates only through Cu material in the peak shocked state (constant state) and does not interact with any other waves before reaching the Cu–LiF interface [Fig. 4(a)]. As a result, no accounting for wave interactions is required—in contrast to the RWO approach. Therefore, for a single shock wave, the FSI approach is quite straightforward and sound speed determination requires only a single Δt measurement, together with the impactor velocity measurement and the Hugoniot relations for Cu (Ref. 9) and LiF,[10] all of which are accurately known. Therefore, we claim that the FSI experiments provide the correct sound speeds for shock compressed Cu.

Hence, the following question arises: Why does the RWO method yield incorrect sound speeds for shock compressed Cu? This question is addressed next.

A. Examination of release wave overtake method for shock compressed solids

To understand the reasons why the RWO results for shock compressed Cu are incorrect, it is necessary to examine the assumptions that govern the RWO method. As discussed in Sec. IV B, the method involves fitting Δt values measured for different sample thicknesses with a straight line and then extrapolating the same to determine the ideal overtake thickness [Fig. 3 (inset) and Fig. 4(e); see also Ref. 24]. However, as noted in Sec. IV B, the validity of this approach depends on several fundamental assumptions and conditions. In particular, a key assumption is that details of the wave interaction [Figs. 4(b)–4(d)] between the right-going release wave in the sample and the left-going reflection from the sample/window interface are independent of the Cu target thickness.

For cases where the shock propagates as a steady single wave and the release occurs along an isentrope in the liquid state, the above assumption is valid. In this case, the right-going release wave and the left-going reflection [Figs. 4(b)–4(d)] both propagate as centered simple waves, where the propagation of each release wave prior to their interaction is self-similar and the flow variables do not depend on distance (x) and time (t) independently, but only on the combination x/t.[44,45] As noted in Sec. IV B, the actual release wave interactions are more complex than shown in Fig. 4. Therefore, a rigorous demonstration of the validity of the RWO method for release along an isentrope—that incorporates the complex release wave interactions—is provided in the Appendix. Also, we emphasize that the validity of the above RWO assumptions is questionable for experiments where the wave profiles display multiple shock waves.

In the present case, where shock compressed Cu is released from the solid state, the validity of the RWO assumptions is not assured because the release path is not along an isentrope due to the Cu elastic–inelastic release response. However, self-similar release wave propagation can be realized in solids, if the following conditions are met: (1) the elastic–inelastic response is time-independent and (2) the entropy change along the release path depends only on the plastic work. In this case, the longitudinal stress is a single valued function of longitudinal strain along the release path, and the governing equations for release wave propagation can be expressed in a form similar to the characteristic equations for isentropic flow.[44,45] Although a detailed proof of the above statements is beyond the scope of this paper, the sufficiency of the above conditions is supported by the numerical simulations presented previously,[23] in which a material model that meets the above conditions (time-independent, elastic–plastic response) was used to calculate the propagation of release waves for a shock compressed solid in a RWO configuration. The calculated wave profiles were analyzed using the RWO method to obtain the calculated sound speeds. These sound speeds matched those determined directly from the propagation of the in-material release wave in the simulations, thus providing validation for the RWO method for this particular case.

B. Numerical simulations for release wave overtake experiments on copper

To examine the effect of release wave interactions in the RWO experiments presented here, numerical simulations were carried out using two different phenomenological material models for shock compressed Cu. The first was a time-independent, elastic-perfectly plastic model[46] that incorporates the linear $U_S - u_p$ relationship from Table II, together with the assumption that the density-Grüneisen parameter product is constant, to determine the mean stress response. The shear modulus was assumed to have a quadratic dependence on the mean stress,

$$G = G_0 + G_1 P + G_2 P^2, \tag{5}$$

and the shear strength was assumed to be constant,

$$Y = Y_0, \tag{6}$$

where Y_0 is the yield stress at the elastic limit. Because this model contains no characteristic length or time scales, release waves calculated using this model exhibit self-similar propagation behavior. As noted above, previous calculations for shock compressed silver[23] using a similar material model have shown results consistent with the RWO method.

The second model incorporates the same mean stress response and the same shear modulus as the first model, resulting in the same elastic response. However, the inelastic response for the second model was determined using the time-dependent or dislocation-based approach from Johnson *et al.*,[47] referred to as the backstress model. This approach—which provides a good match to Cu release wave profiles at low stresses (~20 GPa)[47]—incorporates a quasielastic release response based on the time-dependent behavior of pinned dislocation loops in the early stages of unloading, prior to the onset of large-scale plastic deformation. Because this model incorporates a time-dependent material response, release wave propagation calculated using this model is not consistent with the RWO assumptions presented in Sec. V A.

Figure 6 shows the calculated and measured wave profiles for two FSI experiments (experiments 18 and 19) reaching similar stresses (154 and 156 GPa) but having significantly different impactor thicknesses (907 and 357 μm, respectively). To better compare the wave profiles from the two experiments, the impact surface velocities are normalized by their peak values, and the time axis is normalized by the Cu impactor thickness. The normalized release wave arrival times for the two experiments (black curves) are the same within the experimental uncertainty (see Fig. 5), showing that the sound speed determinations are not significantly dependent on sample thickness. Wave profiles calculated using both the time-independent or elastic–plastic model and the time-dependent or backstress model (red and blue curves, respectively) provide a good match to the measured release wave arrival times, showing that the FSI sound speed determinations are insensitive to the details of the inelastic deformation response. However, we note that the backstress model provides a better overall match to the measured release wave profiles.

The calculated and measured wave profiles for the three sample thicknesses from a representative RWO experiment (experiment 25, reaching 161 GPa peak stress) are shown in Fig. 7(a). Wave profiles calculated using the time-independent or elastic–plastic model do not provide a good match to the measured release wave profiles. In particular, the calculated release wave arrival is too

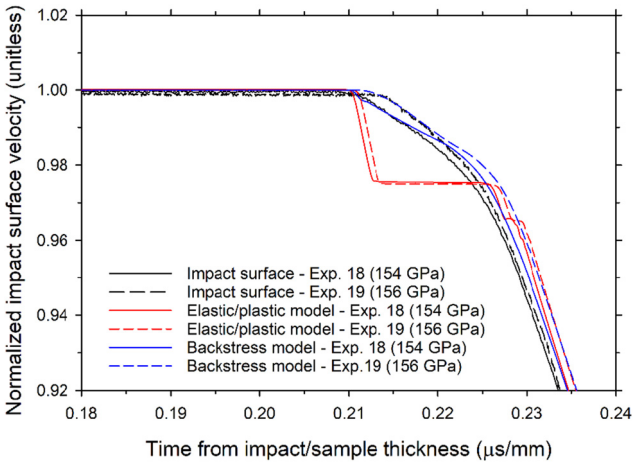

FIG. 6. Calculated and measured wave profiles for two FSI experiments. The solid curves are for experiment 18 (154 GPa) and the dashed curves are for experiment 19 (156 GPa). The black curves are the measured profiles, the red curves are calculated using the elastic/plastic model, and the blue curves are calculated using the backstress model. To better compare wave profiles from the two experiments, the impact surface velocities are normalized by their peak values, and the time axis is normalized by the Cu impactor thickness.

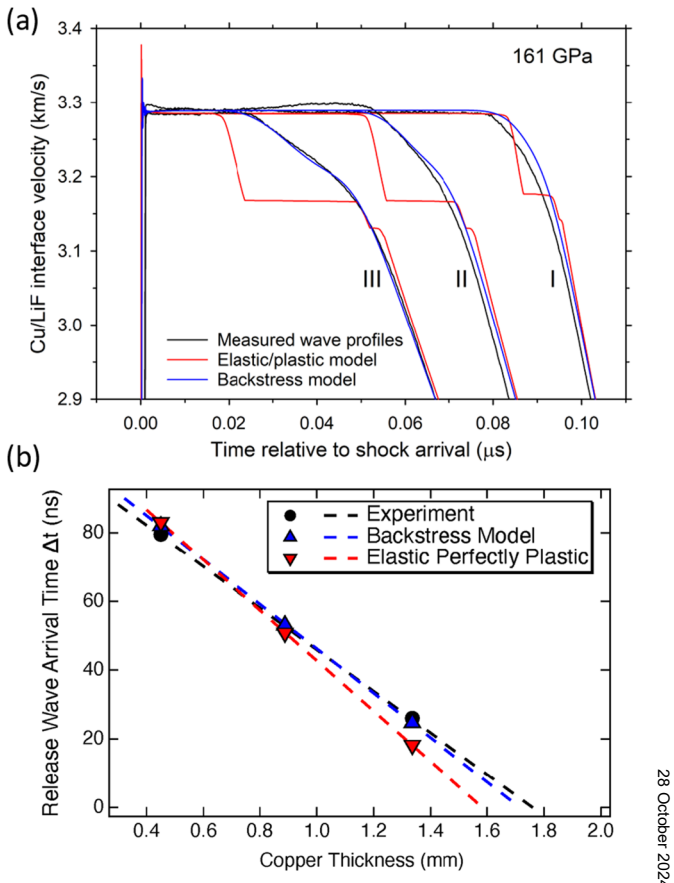

FIG. 7. (a) Calculated and measured wave profiles for a representative RWO experiment (experiment 25). For each profile, time zero denotes shock wave arrival at the Cu/LiF interface. The black curves are the measured profiles, the red curves are calculated using the elastic/plastic model, and the blue curves are calculated using the backstress model. The profiles for the three different target thicknesses are labeled I, II, and III (see Table I). (b) Release wave arrival times (Δt) vs target thickness, showing a straight line fit to determine the ideal overtake thickness. The experimental results are shown in black, results calculated using the elastic/plastic model are shown in red, and the results calculated using the backstress model are shown in blue.

late for the thinnest sample and too early for the thickest sample. In contrast, the backstress model provides a good match to the wave profiles, including the measured release wave arrival times. The good match provided by the backstress model—and not by the elastic–plastic model—demonstrates the importance of the time-dependent quasielastic release response of Cu for understanding the results from the RWO experiments.

The calculated and measured release wave arrival times from Fig. 7(a) are plotted against the target thickness in Fig. 7(b). Because the release wave arrival times calculated using the time-dependent or backstress model agree well with the measured results, the calculated ideal overtake thickness provides a good match to the measured value. In contrast, results calculated using the time-independent or elastic–plastic model result in an ideal overtake thickness that is significantly smaller than the measured RWO result, but is consistent with that expected based on the FSI results.

The results in Figs. 6 and 7 show that the lower sound speeds determined in the RWO experiments, compared to the FSI experiments, arise largely due to the release wave interactions inherent to the RWO method. The time-dependent quasielastic release response of Cu appears to play a central role, leading to violations of the fundamental assumptions underlying the RWO method. Additional theoretical studies are needed to further elucidate the effects of the time-dependent Cu quasielastic response during the interaction of the two release waves.

Although not central to the present study, we provide the following comments regarding the copper response at peak stresses approaching 190 GPa and a calculated temperature of ~4500 K from published theoretical studies.[48] Even at these high stresses and temperatures, copper displays a time-dependent, quasielastic response—observed in metals at lower stresses.[47] Thus, the use of a hydrodynamic or a time-independent elastic–plastic response to model the unloading response of shock compressed copper at these high stresses is not appropriate and the development of a more realistic model for copper to take into account the stress deviators is needed.

C. Copper as a standard for shock compression experiments

Recently, Cu impactors have been incorporated in experiments to determine the sound speeds in shock compressed metals.[30,49] Accurate sound speed determinations in those experiments require

accurate knowledge of the Cu impactor sound speeds. Therefore, the following question arises: What effects do the present differences in Cu sound speeds—determined using FSI or RWO experiments—have on sound speed determinations using experimental configurations that incorporate a Cu impactor? Clearly, the answer to this question depends on the details of the experimental configuration, including the thickness of the Cu impactor compared to that of the sample, and the properties of the sample material. However, some insight can be obtained by considering a specific example from the recent literature—namely, sound speed determination in shocked [100] aluminum single crystals.[49] Using the experimental information from Ref. 49, the [100] Al sound speed at 158 GPa was determined using the Cu impactor sound speeds determined from our FSI results and RWO results. These two determinations result in [100] Al sound speeds that differ by 4.5%. Because this difference is significantly larger than the reported <2% experimental uncertainty,[49] the present findings regarding differences in the measured Cu sound speeds are of significant practical importance.

VI. SUMMARY AND CONCLUSIONS

Longitudinal sound speeds in Cu shock compressed to 190 GPa—where Cu remains in the solid phase—were determined using two different experimental approaches: the front surface impact (FSI) method and the release wave overtake (RWO) method. We find that the sound speeds determined using the two methods diverge significantly for stresses greater than ~100 GPa, with the FSI sound speeds larger than the RWO sound speeds. Due to the lack of wave interactions in the experiments, we believe that the FSI results provide the correct sound speeds for shock compressed Cu. The same is recommended for use in analyzing plate impact experiments that incorporate Cu as a high impedance impactor.

Numerical simulations conducted using two different material models for shock compressed Cu suggest that the lower sound speeds determined in the RWO experiments are due to the effects of the time-dependent Cu quasielastic release response[47] that arise during the release wave interactions inherent to the RWO method. These effects likely result in violations of the fundamental assumptions of the RWO method. Our simulations also suggest that an improved description of the stress deviators during copper release is warranted.

Although the RWO method is generally expected to provide accurate results for solids shock compressed into the liquid phase (shock melting), most of the previous RWO studies involved shock compression over a range of peak stresses that also encompassed peak states in the solid phase.[11,12,23,25–30,38] Therefore, in view of our results for Cu, the previous RWO results for sound speeds in the shock compressed solid phase may need to be reexamined by conducting FSI experiments for direct head-to-head comparisons, similar to the present study.

Previously published data enabling direct comparisons of the FSI and RWO results are available only for tantalum[18,27] and silver.[23] For Ta, comparisons between the FSI results and the RWO results are difficult because the experiments for the two methods were conducted in different studies and the results show significant experimental scatter. For Ag, the FSI and RWO experiments conducted in a single study showed good agreement,[23] in contrast to the present results for Cu. Therefore, the present findings together with the previous results for Ag demonstrate the need to experimentally verify—on a case-by-case basis—the validity of the RWO method for future work on solids shock compressed to stresses below melt.

ACKNOWLEDGMENTS

N. Arganbright is gratefully acknowledged for his expert assistance with the experiments. This work was supported by the U.S. Department of Energy (DOE) National Nuclear Security Administration (NNSA) under Cooperative Agreement No. DE-NA0003957.

AUTHOR DECLARATIONS

Conflict of Interest

The authors have no conflicts to disclose.

Author Contributions

J. A. Hawreliak: Conceptualization (equal); Formal analysis (equal); Investigation (equal); Supervision (equal); Writing – review & editing (equal). **J. M. Winey:** Conceptualization (equal); Formal analysis (equal); Writing – original draft (lead); Writing – review & editing (equal). **Y. Toyoda:** Investigation (equal). **K. Zimmerman:** Investigation (equal). **Y. M. Gupta:** Conceptualization (equal); Supervision (equal); Writing – review & editing (equal).

DATA AVAILABILITY

The data that support the findings of this study are available within the article.

APPENDIX: VALIDITY OF RELEASE WAVE OVERTAKE METHOD FOR MATERIALS HAVING AN ISENTROPIC RELEASE RESPONSE

In the release wave overtake (RWO) method, it is assumed that the measured difference between the arrival time of the right-going shock wave t_S and the onset of the right-going release wave t_R at the sample–window interface can be linearly extrapolated to determine the target thickness at which $\Delta t = t_R - t_S = 0$.[11,24] This condition determines the ideal overtake thickness (Sec. IV B and Fig. 4), from which the sound speed is determined. Here, we provide a rigorous demonstration—not previously available in the literature—that the above assumption for the onset of the release wave is valid for materials having an isentropic release response (e.g., nonviscous fluids). Specifically, we demonstrate that the time interval $\Delta t = t_R - t_S$ for such materials depends linearly on the target thickness, reaching zero when the target thickness reaches the ideal overtake thickness.

The wave propagation encountered for a single sample in an RWO experiment is shown schematically in Fig. 8, where the position coordinate h indicates the Lagrangian position.[44,45] The red curves are shock waves. The black and gray solid lines are the

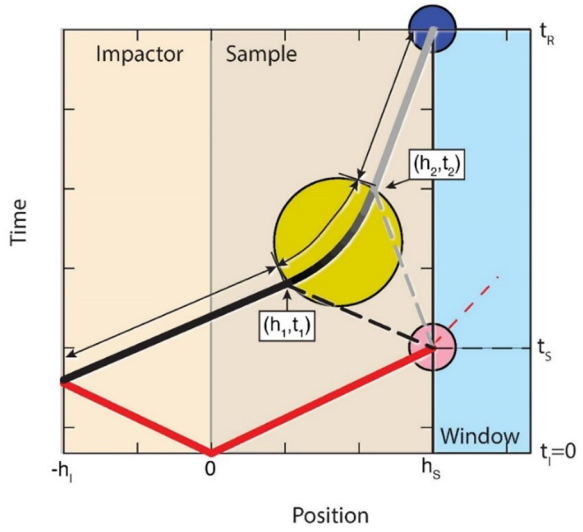

FIG. 8. Time vs distance diagram for a hypothetical RWO experiment where the release response is isentropic. The red lines are shock waves. The black and gray solid lines are the leading edges of the right-going release wave before and after interaction with the left-going release wave, respectively. The black and gray dashed lines are the leading and trailing edges of the left-going release wave fan. The yellow circle indicates the interaction region for the leading edge of the right-going release wave as it interacts with the left-going release wave fan.

leading edges of the right-going release wave before and after interaction with the left-going release wave. The black and gray dashed lines are the leading and trailing edges of the left-going release wave fan. For isentropic flow, the release waves in Fig. 8 propagate as centered simple waves and, therefore, exhibit self-similar wave propagation.[44,45] The waves of interest in Fig. 8 propagate along straight lines (indicating constant velocity) in the $h-t$ plane, except when the two release waves interact with each other in the region bounded by the points (h_1, t_1) and (h_2, t_2). For times prior to t_1, the leading edge of the right-going and left-going release waves (black curves) both propagate at the Lagrangian sound speed c_L for the shocked state. The trailing edge of the left-going release wave propagates at a reduced sound speed c_L^*, as does the right-going release wave for times after t_2 (gray curves).

The time interval of interest, $\Delta t = t_R - t_S$, can be determined by writing it in terms of its constituent time intervals (see Fig. 8),

$$\Delta t = t_R - t_S = \Delta t_{Simp} + \Delta t_{Rimp} + \Delta t_{R1} + \Delta t_{12} + \Delta t_{R2} - t_S, \quad \text{(A1)}$$

where Δt_{Simp} is the transit time of the left-going shock wave in the impactor, Δt_{Rimp} is the transit time of the right-going release wave in the impactor, Δt_{R1} is the transit time of the right-going release wave in the sample from the impact surface to position h_1, Δt_{12} is the transit time of the right-going release wave in the sample from h_1 to h_2, and Δt_{R2} is the transit time of the right-going release wave in the sample from h_2 to the sample–window interface. The validity of the RWO method can be demonstrated by expressing each time interval on the right-hand side of Eq. (A1) in terms of the sample thickness h_S and the ideal overtake thickness h_{ov} (Sec. IV B).

Alternatively, the algebra is considerably simplified by noting that

$$t_R - t_S = 2(t_2 - t_S) = 2\frac{(h_S - h_2)}{c_L^*}. \quad \text{(A2)}$$

Because the left-going release wave fan from the sample–window interface (dashed lines in Fig. 8) is a centered simple wave, the points (h_1, t_1) and (h_2, t_2) must lie on a hyperbola with respect to the centering point (h_S, t_S),[44] resulting in

$$(h_1 - h_S)(t_1 - t_S) = (h_2 - h_S)(t_2 - t_S). \quad \text{(A3)}$$

Combining Eqs. (A2) and (A3) yields

$$t_R - t_S = 2\sqrt{\frac{c_L}{c_L^*}}(t_1 - t_S), \quad \text{(A4)}$$

where we have used

$$c_L = \frac{h_S - h_1}{t_1 - t_S}. \quad \text{(A5)}$$

Considering wave propagation from impact to the point (h_1, t_1) in Fig. 8, we have

$$t_1 = \frac{h_{imp}}{U_S} + \frac{h_{imp}}{c_L} + \frac{h_1}{c_L} = \frac{h_S}{U_S} + \frac{(h_S - h_1)}{c_L}, \quad \text{(A6)}$$

where U_S is the shock velocity. Solving Eq. (A6) for h_1 and introducing the ideal overtake thickness h_{ov} defined by Eq. (3), we obtain

$$h_1 = \frac{c_L}{2}\left[h_S\left(\frac{1}{U_S} + \frac{1}{c_L}\right) - h_{ov}\left(\frac{1}{U_S} - \frac{1}{c_L}\right)\right]. \quad \text{(A7)}$$

Substituting Eq. (A6) into Eq. (A4), and using Eq. (A7), yields

$$\Delta t = t_R - t_S = (h_{ov} - h_S)\sqrt{\frac{c_L}{c_L^*}}\left(\frac{1}{U_S} - \frac{1}{c_L}\right), \quad \text{(A8)}$$

which completes the desired demonstration that Δt is linear in h_S and that Δt goes to zero at the ideal overtake thickness, as required by the release wave overtake method.

We note that the above demonstration is applicable for the experimental approach presented here, which differs somewhat from the RWO approach presented previously.[11,24] However, the corresponding demonstration of validity for the previous RWO approach is similar.

REFERENCES

[1]N. C. Holmes, J. A. Moriarty, G. R. Gathers, and W. J. Nellis, "The equation of state of platinum to 660 GPa (6.6 mbar)," J. Appl. Phys. **66**, 2962 (1989).

[2]A. D. Chijioke, W. J. Nellis, and I. F. Silvera, "High-pressure equations of state of Al, Cu, Ta, and W," J. Appl. Phys. **98**, 073526 (2005).
[3]M. Yokoo, N. Kawai, K. G. Nakamura, K. I. Kondo, Y. Tange, and T. Tsuchiya, "Ultrahigh-pressure scales for gold and platinum at pressures up to 550 GPa," Phys. Rev. B **80**, 104114 (2009).
[4]J. M. Walsh, M. H. Rice, R. G. McQueen, and F. L. Yarger, "Shock-wave compressions of twenty-seven metals. Equations of state of metals," Phys. Rev. **108**, 196 (1957).
[5]R. G. McQueen and S. P. Marsh, "Equation of state for nineteen metallic elements from shock-wave measurements to two megabars," J. Appl. Phys. **31**, 1253 (1960).
[6]R. G. McQueen, S. P. Marsh, J. W. Taylor, J. N. Fritz, and W. J. Carter, "The equation of state of solids from shock wave studies," in *High-Velocity Impact Phenomena* (Academic, New York, 1970), pp. 293–417.
[7]A. C. Mitchell and W. J. Nellis, "Shock compression of aluminum, copper, and tantalum," J. Appl. Phys. **52**, 3363 (1981).
[8]M. D. Knudson and M. P. Desjarlais, "Shock compression of quartz to 1.6 TPa: Redefining a pressure standard," Phys. Rev. Lett. **103**, 225501 (2009).
[9]M. D. Knudson and M. P. Desjarlais, "Adiabatic release measurements in α-quartz between 300 and 1200 GPa: Characterization of α-quartz as a shock standard in the multimegabar regime," Phys. Rev. B **88**, 184107 (2013).
[10]M. D. Knudson, M. P. Desjarlais, and A. Pribram-Jones, "Adiabatic release measurements in aluminum between 400 and 1200 GPa: Characterization of aluminum as a shock standard in the multimegabar regime," Phys. Rev. B **91**, 224105 (2015).
[11]J. M. Brown and R. G. McQueen, "Melting of iron under core conditions," Geophys. Res. Lett. **7**, 533–536, https://doi.org/10.1029/GL007i007p00533 (1980).
[12]J. M. Brown and R. G. McQueen, "Phase transitions, Grüneisen parameter, and elasticity for shocked iron between 77 GPa and 400 GPa," J. Geophys. Res. Solid Earth **91**, 7485, https://doi.org/10.1029/JB091iB07p07485 (1986).
[13]D. E. Grady, W. J. Murri, and P. S. De Carli, "Hugoniot sound velocities and phase transformations in two silicates," J. Geophys. Res. Solid Earth **80**, 4857, https://doi.org/10.1029/JB080i035p04857 (1975).
[14]J. B. Aidun and Y. M. Gupta, "Shear and compression waves in shocked calcium carbonate," J. Geophys. Res. Solid Earth **100**, 1955, https://doi.org/10.1029/94JB02575 (1995).
[15]M. K. Wallace, J. M. Winey, and Y. M. Gupta, "Sound speed measurements in lithium fluoride single crystals shock compressed to 168 GPa along [100]," J. Appl. Phys. **130**, 035901 (2021).
[16]J. A. Hawreliak, J. M. Winey, Y. Toyoda, M. Wallace, and Y. M. Gupta, "Shock-induced melting of [100] lithium fluoride: Sound speed and Hugoniot measurements to 230 GPa," Phys. Rev. B **107**, 014104 (2023).
[17]B. J. Jensen, F. J. Cherne, J. C. Cooley, M. V. Zhernokletov, and A. E. Kovalev, "Shock melting of cerium," Phys. Rev. B **81**, 214109 (2010).
[18]P. A. Rigg, R. J. Scharff, and R. S. Hixson, "Sound speed measurements in tantalum using the front surface impact technique," J. Phys.: Conf. Ser. **500**, 032018 (2014).
[19]M. Lucas, J. M. Winey, and Y. M. Gupta, "Sound velocities in highly oriented pyrolytic graphite shocked to 18 GPa: Orientational order dependence and elastic instability," J. Appl. Phys. **118**, 245903 (2015).
[20]T. J. Volz and Y. M. Gupta, "Elastic moduli of hexagonal diamond and cubic diamond formed under shock compression," Phys. Rev. B **103**, L100101 (2021).
[21]E. J. Berryman, J. M. Winey, Y. M. Gupta, and T. S. Duffy, "Sound velocities in shock-synthesized stishovite to 72 GPa," Geophys. Res. Lett. **46**, 13695, https://doi.org/10.1029/2019GL085301 (2019).
[22]M. T. Beason, B. J. Jensen, and S. D. Crockett, "Shock melting and the hcp-bcc phase boundary of Mg under dynamic loading," Phys. Rev. B **104**, 144106 (2021).
[23]M. K. Wallace, J. M. Winey, and Y. M. Gupta, "Sound speed measurements in silver shock compressed to 300 GPa: Solid-state transition, melting, and liquid-state response," Phys. Rev. B **104**, 214106 (2021).
[24]R. G. McQueen, J. W. Hopson, and J. N. Fritz, "Optical technique for determining rarefaction wave velocities at very high pressures," Rev. Sci. Instrum. **53**, 245–250 (1982).
[25]J. H. Nguyen and N. C. Holmes, "Melting of iron at the physical conditions of the Earth's core," Nature **427**, 339 (2004).
[26]J. M. Brown and J. W. Shaner, "Rarefaction velocities in shocked tantalum and the high pressure melting point," in *Shock Waves in Condensed Matter—1983*, edited by J. R. Asay, R. A. Graham, and G. K. Straub (Elsevier, New York, 1984), pp. 91–94.
[27]M. C. Akin, J. H. Nguyen, M. A. Beckwith, R. Chau, W. P. Ambrose, O. V. Fat'yanov, P. D. Asimow, and N. C. Holmes, "Tantalum sound velocity under shock compression," J. Appl. Phys. **125**, 145903 (2019).
[28]R. S. Hixson, D. A. Boness, J. W. Shaner, and J. A. Moriarty, "Acoustic velocities and phase transitions in molybdenum under strong shock compression," Phys. Rev. Lett. **62**, 637 (1989).
[29]J. H. Nguyen, M. C. Akin, R. Chau, D. E. Fratanduono, W. P. Ambrose, O. V. Fat'yanov, P. D. Asimow, and N. C. Holmes, "Molybdenum sound velocity and shear modulus softening under shock compression," Phys. Rev. B **89**, 174109 (2014).
[30]C. A. McCoy, M. D. Knudson, and M. P. Desjarlais, "Sound velocity, shear modulus, and shock melting of beryllium along the Hugoniot," Phys. Rev. B **100**, 054107 (2019).
[31]P. A. Rigg, M. D. Knudson, R. J. Scharff, and R. S. Hixson, "Determining the refractive index of shocked [100] lithium fluoride to the limit of transmissibility," J. Appl. Phys. **116**, 033515 (2014).
[32]J. M. Winey, M. D. Knudson, and Y. M. Gupta, "Shock compression response of diamond single crystals at multimegabar stresses," Phys. Rev. B **101**, 184105 (2020).
[33]R. G. Kraus, J.-P. Davis, C. T. Seagle, D. E. Fratanduono, D. C. Swift, J. L. Brown, and J. H. Eggert, "Dynamic compression of copper to over 450 GPa: A high-pressure standard," Phys. Rev. B **93**, 134105 (2016).
[34]D. E. Fratanduono, R. F. Smith, S. J. Ali, D. G. Braun, A. Fernandez-Pañella, S. Zhang, R. G. Kraus, F. Coppari, J. M. McNaney, M. C. Marshall, L. E. Kirch, D. C. Swift, M. Millot, J. K. Wicks, and J. H. Eggert, "Probing the solid phase of noble metal copper at terapascal conditions," Phys. Rev. Lett. **124**, 015701 (2020).
[35]S. P. Marsh, *LASL Shock Hugoniot Data* (University of California Press, Los Angeles, 1980).
[36]M. Yokoo, N. Kawai, K. G. Nakamura, and K. Kondo, "Hugoniot measurement by hyper-velocity impact at velocities up to 9 km/s using a two-stage light-gas gun under optimized shot conditions," Int. J. Impact Eng. **35**, 1878–1883 (2008).
[37]C. A. McCoy, M. D. Knudson, and S. Root, "Absolute measurement of the Hugoniot and sound velocity of liquid copper at multimegabar pressures," Phys. Rev. B **96**, 174109 (2017).
[38]D. Hayes, R. S. Hixson, and R. G. McQueen, "High pressure elastic properties, solid-liquid phase boundary and liquid equation of state from release wave measurements in shock-loaded copper," AIP Conf. Proc. **505**, 483–488 (2000).
[39]R. J. Edwards, S. D. Rothman, T. J. Vogler, and M. D. Furnish, "Inferring the high-pressure strength of copper by measurement of longitudinal sound speed in a symmetric impact and release experiment," J. Appl. Phys. **125**, 145901 (2019).
[40]S. M. Sharma, S. J. Turneaure, J. M. Winey, and Y. M. Gupta, "Transformation of shock-compressed copper to the body-centered-cubic structure at 180 GPa," Phys. Rev. B **102**, 020103(R) (2020).
[41]H. M. Ledbetter, "Sound velocities and elastic-constant averaging for polycrystalline copper," J. Phys. D: Appl. Phys. **13**, 1879 (1980).
[42]L. M. Barker and R. E. Hollenbach, "Laser interferometer for measuring high velocities of any reflecting surface," J. Appl. Phys. **43**, 4669 (1972).
[43]O. T. Strand, D. R. Goosman, C. Martinez, T. L. Whitworth, and W. W. Kuhlow, "Compact system for high-speed velocimetry using heterodyne techniques," Rev. Sci. Instrum. **77**, 083108 (2006).

[44]R. Courant and K. O. Friedrichs, *Supersonic Flow and Shock Waves* (Interscience, New York, 1948). Reprint by Springer-Verlag, 1976.
[45]Y. B. Zel'dovich and Y. P. Raizer, *Physics of Shock Waves and High-Temperature Hydrodynamic Phenomena* (Academic, New York, 1966). Reprint by Dover, 2002.
[46]L. E. Malvern, *Introduction to the Mechanics of a Continuous Medium* (Prentice-Hall, Englewood Cliffs, 1969).
[47]J. N. Johnson, R. S. Hixson, G. T. Gray III, and C. E. Morris, "Quasielastic release in shock-compressed solids," J. Appl. Phys. **72**, 429 (1992).
[48]C. W. Greeff, J. C. Boettger, M. J. Graf, and J. D. Johnson, "Theoretical investigation of the Cu EOS standard," J. Phys. Chem. Solids **67**, 2033 (2006).
[49]P. Renganathan and Y. M. Gupta, "Melting anisotropy in crystalline solids," Phys. Rev. B **109**, L060102 (2024).